Rotational Temperature Measurements in Free Jet Expansions of N_2 Using Electron Beam Fluorescence Technique

By

Takeo SOGA*, Masaya TAKANISHI*, and Michiru YASUHARA*

(February 1, 1983)

1. Introduction

The electron beam fluorescence technique has become a standard rotational temperature diagnostics in low density, high-velocity gas flow since it was first demonstrated in the pioneering work by Muntz [1]. The measurement consists of observing the intensity distribution in the rotational structure of the fluorescence created by a high energy electron beam and relating this to the initial population distribution through an appropriate model of excitation-emission process. Application of the Born approximation to the excitation process results in the dipole model used by Muntz.

As the experience with the technique grew [2]–[4], it becomes evident that differences between measured temperature and the calculated temperature were ever-permanent and could not be diminished as random measuring errors. New excitation models which included the effects of the secondary electron excitation were then proposed [5], [6]. Coe *et al* [6] found that the effect of the secondary electrons was insensitive in the variation of density n for $n<1\times10^{16}$ cm^{-3} and proposed the "ejected electron interaction" excitation model (EEI model). In this model, the excitation is consisted of i times quadrupole interactions with the secondary electrons in addition to the initial dipole interaction with the primary electrons. Their measurements with EEI model showed that the rotational temperatures in the nonequilibrium free jet expansions were higher than those in the isentropic expansions, while the rotational energy had a Boltzmann distribution.

In the present report, we show the results of measurements of the rotational temperature along the center-line of free jets (Fig. 1) from the orifice exit to far downstream of the first Mach disc and examine the Muntz's excitation model and EEI

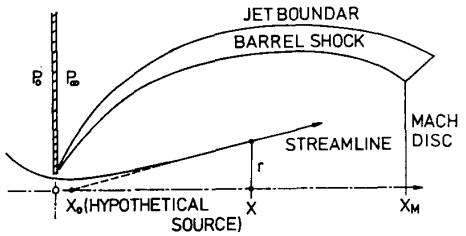

Fig. 1. Sketch of free jet flow field.

* Present address: Japan Airline, Ota-ku, Tokyo.
Department of Aeronautical Engineering, Nagoya University

This document is provided by JAXA.

model. We also show the numerical solutions of the spherical source flow expansions. A comparison of the experimental results with those of kinetic theory will give knowledge of the rotational collision number for nitrogen in low temperature.

2. Experimental Apparatus

The low density chamber with 1 m in diameter and 1.6 m in length, is a continuous running facility having a pumping system of a 14″ oil vapor diffusion-ejector pump; the maximum pumping speed is 4000 liters/sec. at chamber pressure, P_∞, about 1×10^{-3} Torr. This pump is connected to a 5HP oil rotary pump that has a 3900 liters/min. pumping capacity [7]. The free jets were issued from a converging nozzle or a orifice attached to the side of the plenum chamber (10 cm in diameter and 13 cm in length) which was mounted on the two-dimensional traverse in the low density chamber.

The maximum pumping speed of the systems was 100 Torr-mm in the scale of P_0D where P_0 is the stagnation pressure and D the diameter of the nozzle exit or the orifice at $P_\infty=3\times10^{-2}$ Torr and 40 Torr-mm at $P_\infty=5\times10^{-3}$ Torr. The jet Reynolds number for N_2 to the sonic condition (the stagnation temperature was 20°C) was $Re^*=20.4\times P_0D$ (Torr-mm).

The electron beam generated by the electron gun (EBW, S/N 522 type) passed through the aperture (3 mm in diameter and 4 mm in thickness) bored on the bottom of the gun chamber. A 6″ oil diffusion pump maintained the gun chamber pressure less than 2×10^{-4} Torr. The electron beam passing through the test gas was collected by a Faraday cage and the beam current was obtained by measuring the voltage drop across a 10 ohm resistance inserted between the Faraday cage and the earth.

The alignment of the electron beam was achieved by a set of electromagnetic deflection coils which were mounted below the electron gun. Then, the electron beam was focused by an electromagnetic lens on the center-line of the free jet, which was done by setting a removable plate at the hight of the center-line; the diameter of the focused electron beam on this plate was about 1.6 mm. The cathode potential and the beam current were held at −15 Kv and 2 mA (measured at the Faraday cage), respectively, and the anode was kept at the ground potential.

For the measurement of the rotational spectrums, a fluorescence from the electron beam was gathered and made parallel by the first lens in the chamber, which was further focused on the entrance slit of the spectrometer (Jarell-Ash 78-490 type, the grating with 1180 rulings/mm, f/6.5) by the second lens in front of the slit (Fig. 2). The second order spectrums with the dispersion of 4.7A°/mm were used. The entrance slit width was about 0.07 mm and the hight was 0.5 mm, while the width of the exit slit was same as the entrance slit width.

Line intensities were measured by a cooled HTV R106UH type hotomultiplyer, having S-19 spectral response. The dark current measured as the noise of the output current was less than 0.2 nA at 750 v when the photomultiplyer was cooled to −15°C. The output of the photomultiplyer was amplified and recorded on the X-T

This document is provided by JAXA.

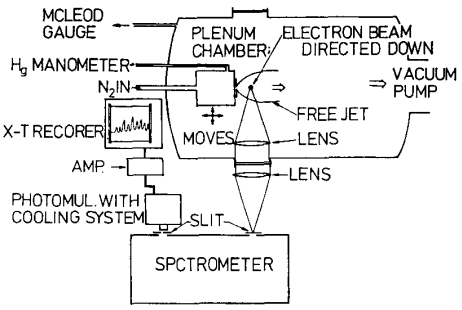

Fig. 2. Top view schematic of the optical system.

recorder against the wave length, i.e., the rotation of the grating.

3. Electron Beam Fluorescence Technique

The energetic electron excites and ionizes the ground state nitrogen molecules ($N_2X^1\Sigma_g^+$) up to the excited state of the molecular ion ($N_2^+B^2\Sigma_u^+$). The subsequent emission to the ground state ion ($N_2^+X^2\Sigma_g^+$) then compries the first negative system [1]. The excitation emission path is indicated schematically in Fig. 3.

For a gas in thermal equilibrium, the population N_K of the K rotational level in the v'' vibrational level is proportional to

$$N_K \infty (2K+1) \exp[-K(K+1)(B_{v''}hc)kT_{rot}]$$

where $B_{v''}$ denotes the molecular rotational constant, h Plank's constant, and c the speed of light. Here, the quantum number J is replaced by K, a quantum number of the rotation of nuclei [1]. At room temperature of less, there is no vibrational excitation of importance in the case of nitrogen, i.e., $v''=0$. The combination $B_0hc/k=\Theta_{rot}$ is the characteristic rotational temperature of the molecule; for nitrogen molecule, $\Theta_{rot}=2.8786$K [8].

If the assumption is made that the ground state nitrogen molecules before excitation has a Boltzmann distribution of the rotational energy at a rotational tempera-

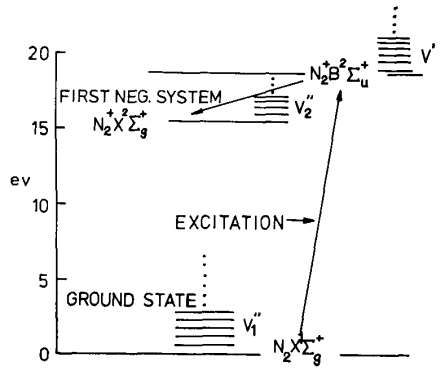

Fig. 3. Excitation and emission paths for the first negative system of nitrogen.

This document is provided by JAXA.

ture T_{rot} and that the excitation from $N_2X^1\Sigma$ to $N_2^+B^2\Sigma$ $(K'\rightarrow K'')$ is governed by the optically allowed selection rule (direct excitation, i.e., the dipole model), the line intensity of 0-0 vibration-rotation band is given by [1]

$$(I_{K'K''})_{v'v''}=C(K'+K''+1)[G](\nu/\nu_0)^4\exp[-K'(K'+1)(\Theta_{rot}/T_{rot})] \qquad (1)$$

where C is a constant, ν the wave number of the emission, and ν_0 a wave number of reference. The factor $[G]$, which includes the Hönl-London rotational transition probability, is given as [1]

$$[G]=\frac{(K'+1)\exp[-2(K'+1)(\Theta_{rot}/T_{rot})]+K'\exp[2K'(\Theta_{rot}/T_{rot})]}{2K'+1}$$

In the optically allowed transition, $\Delta K=K'-K''=\pm 1$, which results in the formation of P-branch ($\Delta K=-1$) and R-branch ($\Delta K=+1$) in the rotational structure. For the 0-0 band in the first negative system, the band origine ($\Delta K=0$) is at 3909 A° and the band head due to the folding back of the P-branch lies at 3914 A°.

Equation (1) is rewritten as

$$\log\left\{\frac{(I_{K'K''})_{v'v''}}{(K'+K''+1)[G](\nu/\nu_0)^4}\right\}=-(\Theta_{rot}/T_{rot})K'(K'+1)+\text{const.} \qquad (2)$$

Plotting the lefthand-side of Eq. (2) versus $K'(K'+1)$, will yield straight line with a slope, Θ_{rot}/T_{rot}, from which T_{rot} is obtained. Since $[G]$ includes T_{rot}, the procedure is iterative.

On the other hand, for EEI model, $[G]$ is given by

$$[G(K')]=\sum_{k=0}^{\infty}{}_KE_{K'}B_K(T_{rot})/B_{K'}(T_{rot});$$

$$B_K(T_{rot})=(2K+1)\exp[-K(K+1)(\Theta_{rot}/T_{rot})],$$

where $\boldsymbol{E}=\{{}_KE_{K'}\}$ is a matrix of transition probabilities from the rotational level K in the $N_2X^1\Sigma$ state to K' in the $N_2^+B^2\Sigma$ state. The matrix element ${}_KE_{K'}$ includes the probability p_i that the overall interactions will be consisted of i quadrupole

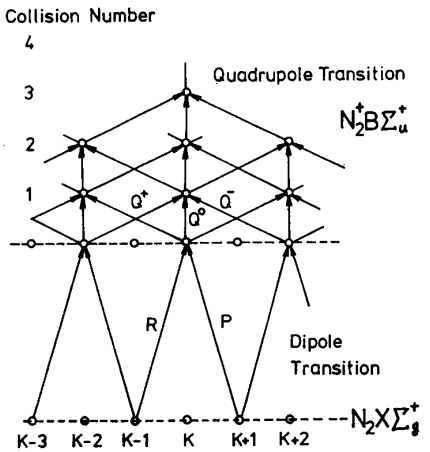

Fig. 4. Excitation paths of the EEI model.

This document is provided by JAXA.

interactions in addition to the initial dipole interaction with the primary electrons. The quadrupole interactions, thus, have the effect of allowing $\Delta K=\pm 3, \pm 5, \ldots,$ transitions (Fig. 4); all elements corresponding to the even value of ΔK are zero on the symmetric ground [8]. Coe *et al.* evaluated p_i empirically [6].

4. Experimental Results

The rotational temperature distribution along the center-line of the free jet from several nozzles and/or orifices were measured. Important flow parameters of the N_2 free jet runs are given in Table I. The spectral data were analyzed in the way as mentioned in Sec. III and the rotational temperatures were obtained. The beam current was continuously monitored to ensure a variation of less than 5% in the beam current during the grating scan. Intensities of the rotational spectrums must have had 5% relative errors at most but the log slope technique may have diminished effects of these errors on the rotational temperature. The accuracy of the position was of the order of 0.5 mm. The stagnation temperature was continuously measured using a copper-constant thermocouple during the run and the variations of it were within 2 K, which was comparative with the variation of room temperature.

A number of log slopes plots for $P_0D=30.0$ Torr-mm are presented in Fig. 5 for various values of x/D where the data were reduced with the dipole model. The data for large value of x/D do not fall on the straight line and show non-Boltzmann distribution of the rotational energy. In Figs. 6-a to 6-f are shown log slopes plots for $P_0D=44.6$ Torr-mm where the open circles are the data reduced with the dipole model and the triangles are those reduced with the EEI model. The data reduced with the EEI model fall on a straight line for $x/D<18.2$, while the data reduced with the dipole model show nonlinear distributions. For $x/D \gtrsim 18.2$, however, the both data do not fall on the straight lines (Figs. 6-d and 6-e). At far downstream (Fig. 6-f), the data fall on the straight line again (which means that gas was in equilibrium).

In Figs. 7-a and 7-b are shown the rotational temperature distributions for P_0D

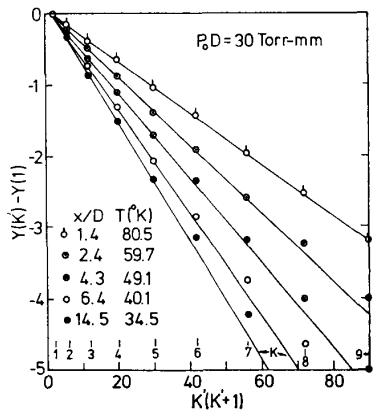

Fig. 5. Log slope plots for $P_0D=30.0$ Torr-mm.

This document is provided by JAXA.

=20.6 and 30.0 Torr-mm, respectively, where the data were reduced by the dipole model because the rotational temperature did not decrease so much in the expansions. The slope of a linear portion of log plots was used to evaluate the temperature. When nonlinearilies appeared in the log plots for small values of K', the slopes were found by the least square fit method, using the first 6 points ($K'=1$ to 6).

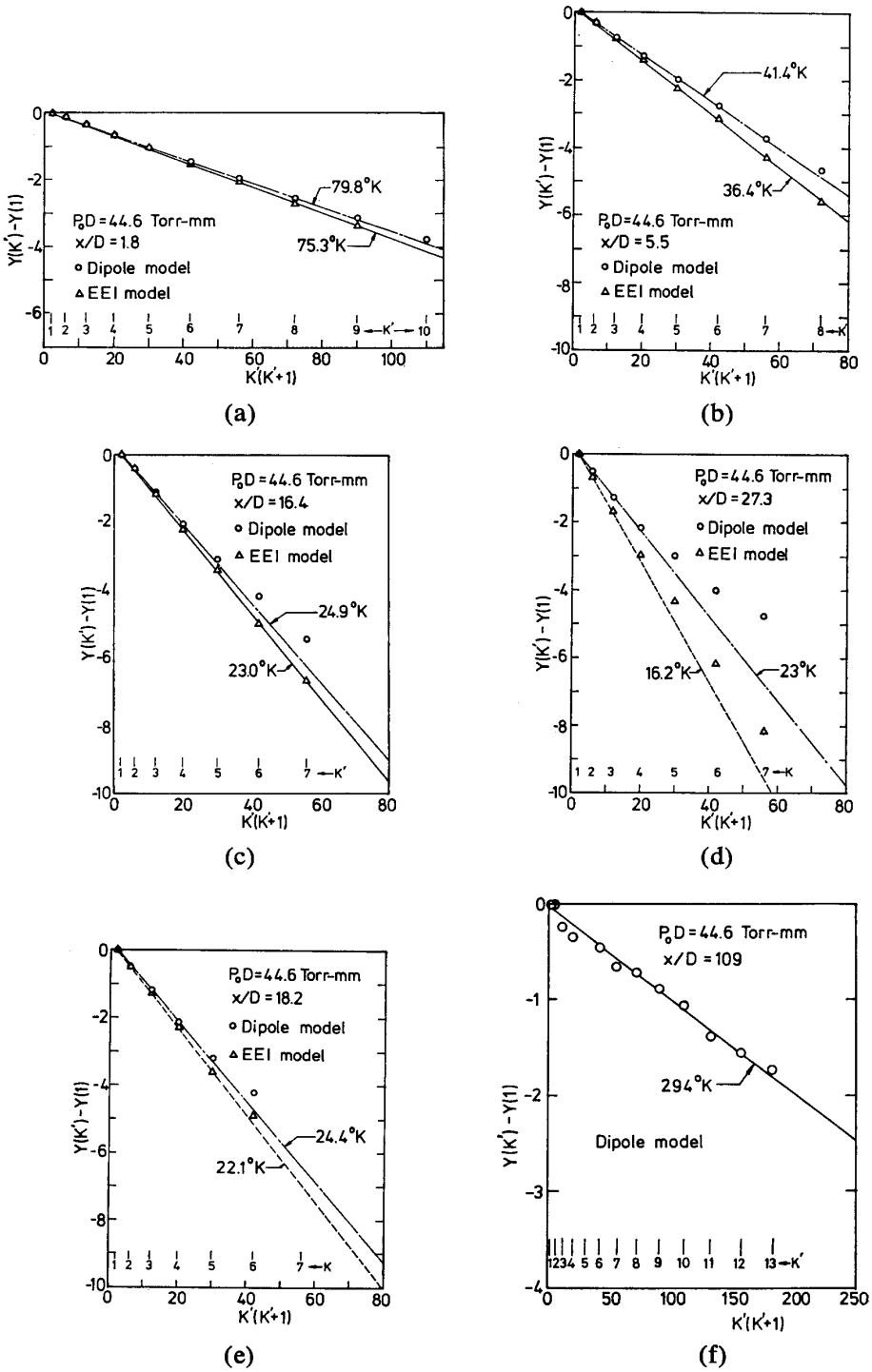

Fig. 6. Log slope plots for P_0D=44.6 Torr-mm.

This document is provided by JAXA.

The rotational temperature was obtained by the three different ways for the cases P_0D=44.6 and 100 Torr-mm; the temperature presented by open circles were obtained by the six points least square fit method (dipole model), the data shown by closed circles were obtained by the first linear portion of the log plots, and the data expressed by triangles were obtained by the slopes of the log plots using the EEI model. For the case P_0D=100 Torr-mm (Fig. 7-d), the measured temperature shows downward deviation from the isentropic one. The measuring points might be a little off-centered from the jet center-line (the diameter of the electron beam was large than the orifice diameter, 0.5 mm). Such off-centered measurement is significant in the vicinity of the orifice exit but it dose not matter to the measurement in the

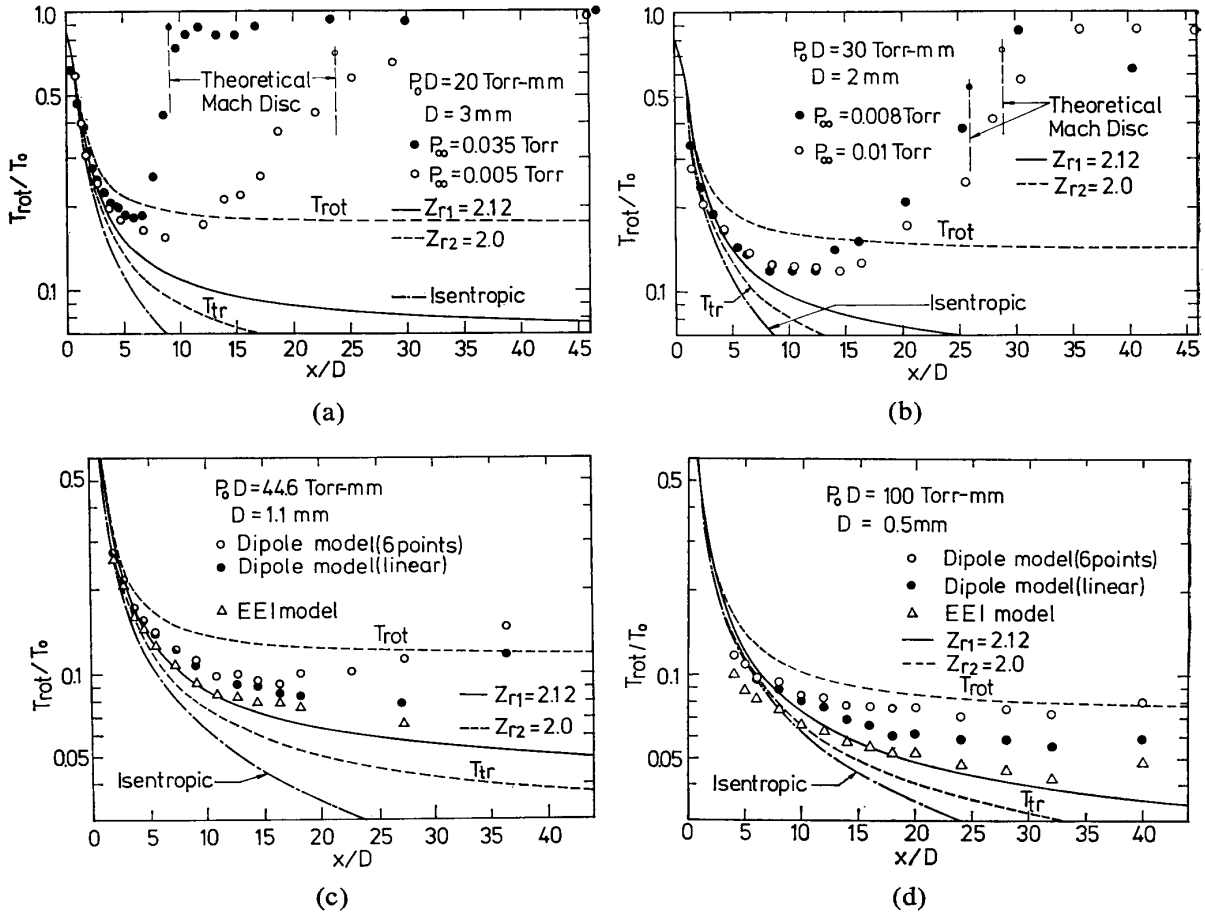

Fig. 7. Rotational temperature distributions along the center-line of free jets.

Table I. Nitrogen free jet flow conditions

P_0D (Torr-mm)	D (mm)	P_0 (Torr)	P (mTorr)	Re^*	X_M/D	T_0 (K)
20.1	3	6.8	35	410	9.3	286
20.1	3	6.8	5	410	24.7	294
30.2	2	15.1	8	615	29.1	293
30.0	2	15.0	10	611	25.9	292
44.6	1.1	40.5	4.5	909	63.6	293
100.0	0.5	200.0	5	2038	134	289

This document is provided by JAXA.

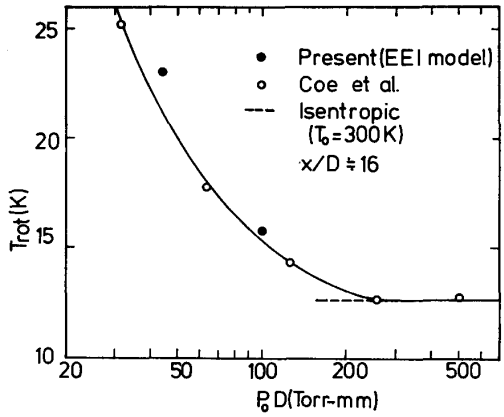

Fig. 8. Rotational temperature at $x/D=16$ vs P_0D.

downstream because the variation of temperature in the radial direction is small [3].

The measured values T_{rot} fall on the isentropic temperature curve for $\gamma=1.4$ at small values of x/D (except for the case of $P_0D=100$ Torr-mm). They show a gradual departure from this curve (Fig. 7-c and 7-d) or a formation of shock wave (Fig. 7-a and 7-b); the effect of Mach disc reaches to the upstream of the theoretical location of it. A comparison of the log slopes plots in Fig. 6 and the rotational temperature distributions in Fig. 7 suggests that if the log plots data reduced with the EEI model show nonlinear features, the nonequilibrium of shock wave (Mach disc) emerges in the data.

In Fig. 8, the rotational temperature at $x/D \fallingdotseq 16$ is plotted vs P_0D where the data of Coe *et al.* [6] are also presented for the comparison. The effect of the increasing rarefaction is to increase the indicated temperature, while the EEI model provides a linear fit of the data of the rotational line intensities (Fig. 6-d); the rotational energy has a Boltzmann distribution corresponding to a nonisentropic temperature.

5. Discussion

As noted in Sec. IV, the effect of the interference of Mach disc emerges in the log plots of the rotational line intensities. Thus, it can be said that the measurement in the upstream of the interference region gives the rotational temperature in the "underexpanded jet". The comparison of the data reduced with the EEI model in Fig. 6 with the same data reduced according to the dipole model illustrates the deg ree of improvement of the EEI model.

It is interesting to know whether or not the resulting rotational temperature is consistent with the theoretically evaluated one. Assuming that the flow near the center-line of the jet is well approximated as a hypersonic spherical expansion flow, Morse's [9] model equation for diatomic gas in the dimensionless form is given by

$$v_r\frac{\partial f^l}{\partial r}+\frac{v_\theta^2+v_\varphi^2}{r}\frac{\partial f^l}{\partial v_r}-\frac{v_r v_\theta}{r}\frac{\partial f^l}{\partial v_\theta}-\frac{v_r v_\varphi}{r}\frac{\partial f^l}{\partial v_\varphi}=J^l;$$
$$J^l=(M_{el}^l-f^l)/(\tau_{el}/\tau_0)+(M_{in}^l-f^l)/(\tau_{in}/\tau_0), \qquad (3)$$

This document is provided by JAXA.

in the spherical coordinates where f^l is the velocity distribution function of the lth rotational energy level, τ_{el} the mean time for elastic collision, τ_{in} the mean time for inelastic collision, and τ_0 is defined by

$$1/\tau_0=1/\tau_{el}+1/\tau_{in}=nkT/\mu,$$

where μ is the shear viscosity of nitrogen.

Elastic and inelastic emission terms M_{el} and M_{in} are given by

$$M_{el}=n(\pi T_{tr})^{-3/2}\exp[-(\boldsymbol{v}-\boldsymbol{u})^2/T_{tr}-E_l/T_{tot}]/\Omega(T_{rot}),$$
$$M_{in}=n(\pi T)^{-3/2}\exp[-(\boldsymbol{v}-\boldsymbol{u})^2/T-E_l/T]/\Omega(T),$$

where T_{tr} is the translational temperature, E_l the energy of the lth energy level, and Ω is the partition function of the rotational mode.

The rotational collision number is given by [10]

$$z_{r1}=(4P\tau_r/\pi\mu)$$

where τ_r is the real relaxation time of rotational energy given by $\tau_r=(5/3)\tau_{in}$. Another definition of Z_r [10], [11] is given by

$$z_{r2}=(4P\tau_r/\pi\mu_h)\ ;\ \mu_h=(5/16\sigma_t^2)(kmT/\pi)^{1/2},$$

where σ_t is an effective hard-sphere diameter for inelastic collision and m the mass of nitrogen molecule. When z_{r1} is constant, z_{r2} is inversely proportional to $T^{1/2}$ and it increase as T decreases. The shear viscosity of nitrogen was evaluated for the Lenard- Johns potential [12].

Equation (3) was solved by a similar manner as the one in refference [13] and the detail of the calculation was shown in reference [14]. The results for $z_{r2}=2$ are shown in Figs. 7-a to 7-d by the broken line. The rotational temperature levels off somewhat suddenly and the translational temperature shows a significant departure from the rotational temperature. The experimental results do not agree with the calculated results even if P_0D is small. The solid line in these figures are results for the case, $\tau_{in}/\tau_0=1$, which gives $Z_{r1}=2.12$; in this case, the translational temperature is nearly equal to the rotational tempera. The agreement with the experimental results is fairly well and the value, $Z_r=2.12$ is consistent with the results of Coe *et al.* [6] and that of Willis *et al.* [15].

The rotational temperature at $x\to\infty$ was measured or estimated by many authors [10], [11], using the time of flight method of the molecular beam. In these experiments, measured rotational temperatures seem to level off to higher values than the present results. As shown in Sec. IV (Fig. 12-a), however, the effect of Mach disc reaches to considerable upstream of the theoretical location of it, at least when the ambient pressure is in the range of 10^{-3} Torr. Thus, it is hoped that the measurements are carried out for various values of x/D, using this method.

This document is provided by JAXA.

6. Smmary

The rotational nonequilibrium has been investigated in the underexpanded free jet of nitrogen, using the electron beam fluorescence technique. The results have shown that the ejected electron interaction excitation model with assumed Boltzmann distribution of ground-state molecules was consistent with the measured line intensities of rotational spectrums in the pure expansion region, while the dipole excitation model was not consistent with the measurements, especially, for high rotational levels. The rotational temperature obtained using the ejected electron excitation model were well correlated with the results obtained by a kinetic analysis of spherical source flow expansions and a comparison of the results indicates a rotational collision number of 2.12.

Acknowledgement

The present work was partly supported by the Scientific funds of the Ministry of Education, and the numerical calculations were carried out using the FACOM M-200 computer at the Computer Center of Nagoya university.

References

[1] E. P. Muntz: Phys. Fluids, **5**, 80 (1962).
[2] F. Robben and L. Talbot: Phys. Fluids, **9**, 644 (1966).
[3] P. V. Marrone: Phys. Fluids, **10**, 521 (1967).
[4] H. Ashkenas: Phys. Fluids, **10**, 2509 (1967).
[5] R. B. Smith: in Rarefied Gas Dynamics, ed. by L. Trilling and H. Y. Wachmann (Academic Press, New York, 1969), Vol. II, p. 1749.
[6] D. Coe, F. Robben, L. Talbot, and R. Cattolica, Phys. Fluids, **23**, 706 (1980).
[7] T. Soga, M. Takanishi, and M. Yasuhara: Memoirs of the Faculty of Engineering, Nagoya Universiıy, Vol. 33, No. 1. May 1981, p. 76.
[8] G. Herzberg: "Molecular Spectra and Molecular Structure", (D, Van Norstrand, Primceton, 1964).
[9] T. F. Morse: Phys. Fluids, **7**, 159 (1964).
[10] R. J. Gallagher and J. B. Fenn: in Rarefied Gas Dynamics, ed. by M. Becker and M. Fiebig (DFVLR-Press, Porz-Wahn, West Germany, 1974), Vol. I, p. B19-1.
[11] P. Poulsen and D. R. Miller, in Rarefied Gas Dynamics, ed. by Potter (Progress in Astronautics and Aeronautics, Vol. 51), (AIAA, 1977), Part II, p. 899.
[12] R. C. Reid and T. K. Sherwood: "The Properties of Gases and Liquids", (MacGraw-hill, 1966).
[13] T. Soga and H. Oguchi: Phys. Fluids, **15**, 766 (1972).
[14] K. Niwa: The Master's thesis, the Faculty of Engieering, Nagoya university (1978).
[15] D. R. Willis and B. B. Hamel: in Rarefied Gas Dynamics, ed. by C. L. Brundin (Academic Press, New York, 1967), Vol. I, p. 837.

This document is provided by JAXA.